Tailoring the Surface Chemical Reactivity of Transition-Metal Dichalcogenide PtTe2 Crystals

A. Politano[1,*], G. Chiarello[2,*], C. N. Kuo[3], C. S. Lue[3], R. Edla[4], P. Torelli[4], V. Pellegrini[1], and D. W. Boukhvalov[5,6,*]

1 Fondazione Istituto Italiano di Tecnologia, Graphene Labs, via Morego 30, 16163 Genoa, Italy
2 Università della Calabria, Dipartimento di Fisica, via ponte Bucci cubo 31/C, 87036 Rende, Cosenza, Italy
3 Department of Physics, National Cheng Kung University, 70101 Tainan, Taiwan
4 Consiglio Nazionale delle Ricerche (CNR)- Istituto Officina dei Materiali (IOM), Laboratorio TASC in Area Science Park S.S. 14 Km 163.5 34149 Trieste, Italy
5 Department of Chemistry, Haiyang University, 17 Haengdang-dong, Seongdong-gu, Seoul 133-791, South Korea
[6] Theoretical Physics and Applied Mathematics Department, Ural Federal University, Mira Street 19, 620002 Ekaterinburg, Russia

Introduction

Graphene is having a groundbreaking impact on science and technology,**1**-**3** owing, in particular, to the high mobility of its charge carriers, together with its flexibility, high specific surface area, and thermal conductivity.**4** After the advent of graphene, an abundant number of 2D materials,**5**, **6** together with their heterostructures,**7**, **8** have attracted the interest of the scientific community, due to their application capabilities, which are often superior to those of graphene.**9** Moreover, many layered materials also exhibit topological properties with implications for various disciplines.**10**, **11**

It is now established that several classes of innovative materials still present drawbacks for technological applications for different motivations: silicene**12** and germanene**13** cannot be exfoliated; MoS_2 has a fairly low mobility of charge carriers;**14** black phosphorus is unstable toward surface oxidation,**15** while bismuth chalcogenides are excessively fragile with uncontrolled formation of fractures.**16** Indeed, chemical inertness is a crucial requirement for a novel material at the basis of potential disruptive technologies.**17** Ambient stability implies the possibility to fabricate nanodevices without any capping layer on the active channel with subsequent easiness for the nanofabrication process and higher prospect for scaling up.**17**

Recently, the PtX_2 (X = S, Se, Te) class has emerged as one of the most promising among layered materials "beyond graphene."**11**, **18**-**21** The high room-temperature (RT) electron mobility,**18** for example, combined with energy-gap tunability upon thickness reduction might enable the fabrication of field-effect transistors to be employed in optoelectronics**18** and gas sensing.**22** Among the PtX_2 class, $PtTe_2$, in particular, has been predicted to exhibit the best performance for hydrogen evolution reaction (HER),**23** which is even further enhanced by oxidation.**24**

The current interest toward this class of materials is further motivated by the existence of bulk type-II Dirac fermions, arising from a tilted Dirac cone.**25**, **26** Type-II Dirac fermions have been experimentally observed in $PtSe_2$**25** and $PtTe_2$.**27** However, contrary to $PtSe_2$ (see Section S1, Supporting Information), $PtTe_2$ can be grown as bulk crystals with excellent crystalline quality and, accordingly, the potential impact of $PtTe_2$ for technology could be even higher than $PtSe_2$.

Bulk $PtTe_2$ is a semimetal with a pair of strongly tilted Dirac cones along the Γ-A direction,**27** which provide massless charge carriers with ultrahigh mobility. $PtTe_2$ crystallizes in the trigonal CdI_2-type crystal structure (see **Figure 1**a,b). The Pt atom is surrounded by six Te atoms, constructing the $PtTe_6$ octahedra along the basal plane. The octahedra link at their edges to form infinite sheets. The adjacent sheets are separated by van der Waals gaps and weak interlayer interaction.

Information on the ambient stability of $PtTe_2$ is a crucial step in order to evaluate the feasibility of its exploitation in technology. Moreover, the possibility to tune surface chemical reactivity by appropriate surface modification is an essential step for its employment for diverse applications, especially in catalysis.

Herein, we present a joint experimental and theoretical investigation of the reactivity of the $PtTe_2$ surface toward most common ambient gases (oxygen and water). We find that bulk stoichiometric $PtTe_2$ single crystals are completely inert toward ambient gases. On the other hand, the presence of defects drives the formation of tellurium-oxide phases. Therefore, the presence of Te vacancies is detrimental for the ambient stability of uncapped $PtTe_2$-based devices. When the surface is modified by the presence of carbon atoms, $PtTe_2$ is transformed into a catalyst. In particular, experiments and theory demonstrate the stable adsorption of hydroxyl groups at RT, which represents an essential step for water splitting and water–gas shift reactions.

Result and discussion

Figure 1a,b displays the crystal structure of $PtTe_2$. Single crystals of $PtTe_2$ were prepared by the self-flux method, as described in the Experimental Section. Their structure has been checked with X-ray diffraction (XRD, Figure S1, Supporting Information). The surface of the cleaved samples exhibits superb flatness, as evidenced by the sharp and bright spots in the low-energy electron diffraction (LEED) pattern (Figure 1c) with suppressed background and with outstanding electron reflectivity. Consequently, the amount of defects of the pristine $PtTe_2$ sample is appraised to be negligible.

To assess the surface chemical reactivity of $PtTe_2$, we have performed high-resolution X-ray photoelectron spectroscopy (XPS) experiments (**Figure 2**). We focused first on the evolution of Pt 4f and Te 3d core levels upon various treatments (O_2 dosage and air exposure), as compared to spectra acquired for the pristine $PtTe_2$.

From the analysis of Te 3d core-level spectra (Figure 2a), we infer that the as-cleaved undefected $PtTe_2$ surface is inert to oxygen exposure. As a matter of fact, only $3d_{5/2}$ and $3d_{3/2}$ core levels at the binding energies of 573.1 and 583.5 eV, corresponding to an oxidation state Te(0), are observed in Figure 2a for both the pristine $PtTe_2$ (red curve) and the same surface exposed to a dose of 10^6 L (1 L = 1.33×10^{-6} mbar s) of O_2 at RT (dashed blue curve).

In the evaluation of the ambient stability of $PtTe_2$, the possible influence of Te vacancies on surface chemical reactivity deserves particular attention. As a matter of fact, Te vacancies may appear on nonstoichiometric samples during the growth process or, alternatively, by implanting defects with preferential sputtering of heavier Pt atoms (compared to Te atoms). To check the influence of Te

vacancies on ambient stability of $PtTe_2$, we have purposefully introduced Te vacancies in stoichiometric $PtTe_2$ samples by Ar-ion sputtering at high kinetic energy (2–4 keV) with a fluence of 10^{16} ions cm^{-2}, as also confirmed by Auger electron spectroscopy (see Section S4, Supporting Information), which has also been used to quantity the amount of Te vacancies.

After exposing to O_2 the $PtTe_2$ surface defected by ion sputtering (Figure 2b, black curve), with a Pt:Te ratio of 39:61, two novel components appear in the Te 3d core levels at higher binding energies, that is, 576.0 and 586.4 eV. These components (highlighted with vertical dashed lines in Figure 2b) are assigned to the Te (IV) species, arising from the formation of Te□O bonds in a tellurium-oxide phase.**28** The intensity of these peaks increases by increasing the amount of the Te vacancies, as shown in Figure S5 (Supporting Information), related to the case of a $PtTe_2$ sample with Pt:Te ratio of 43:57. The Te(IV) components are the most intense lines in the Te 3d XPS spectra for the case of air-exposed defected samples (Figure 2b, yellow curve).

The Pt 4f doublet also reported in Figure 2 is observed at binding energies of 72.5 ($4f_{7/2}$) and 75.9 ($4f_{5/2}$) eV, respectively. Similar values of the binding energy for Pt-4f core levels have been reported for $PtSe_2$.**19**, **29** After various treatments, the Pt 4f core-level spectra did not show any noticeable changes in the binding energies, mostly retained in the Pt(0) configuration. Only a small component at lower binding energy appears in the Pt 4f doublet after the formation of defects on the $PtTe_2$ surface (as highlighted in Figure S3, Supporting Information), in agreement with the observed oxidation of Te, evident from the analysis of Te-3d core levels in Figure 2b. We conclude from the results of the XPS measurements shown in Figure 2 that the implantation of defects drastically changes the reactivity of $PtTe_2$ and, in particular, that TeO_2-like structures are formed in the case of heavily defected $PtTe_2$.

In order to further explore the surface chemical reactivity in $PtTe_2$-based systems, we have also carried out vibrational experiments by means of high-resolution electron energy loss spectroscopy (HREELS). Specifically, we have exposed to water and oxygen (i) pristine (undefected) $PtTe_2$, (ii) $PtTe_2$ surfaces modified by implantation of defects via Ar-ion bombardment, and (iii) C-doped $PtTe_2$. The corresponding vibrational spectra are shown in **Figures 3**–**5**. For the case of pristine (undefected) $PtTe_2$, the vibrational spectrum remains featureless even after exposure of water and oxygen at RT (Figure 3a). Likewise, no vibrational peaks are revealed in the air-exposed undefected $PtTe_2$ surface (blue curve in Figure 3a). Combined with the XPS results reported in Figure 2a,b, these data lead to the conclusion that undefected $PtTe_2$ does not react at RT with ambient gases. This finding has a particular interest in view of applications in optoelectronics based on $PtTe_2$.

Upon heating the surface at 600 K in an oxygen environment (partial pressure of 5×10^{-6} mbar for 1 h), a surface-oxide phase appears. Its loss spectrum is characterized by a very intense and broad vibrational band. A fitting procedure (Figure 3b) allows distinguishing two components, centered at 61 and 94 meV, respectively. Based on XPS results (Figure 2) and the theoretical model describing the early stage of surface oxidation (Section S6, Supporting Information), we attribute these two vibrational components to libration and stretching vibrations of a surface TeO_2 phase,**30** respectively.

The defected sample has a featureless vibrational spectrum (Figure 4a), but upon exposure to O_2 at RT a broad vibrational band appears, with two different components at 80 and 105 meV, respectively (see fitting procedure in Figure 4b). While the mode at 80 meV is easily assigned to the O-O stretching vibration,**31** the origin of the vibration at 105 meV is unveiled by performing a similar investigation on $PdTe_2$, for which we find the same vibrational mode (Figure S5, Supporting Information). Therefore, the feature at 105 meV is evidently Te-related rather than Pt-derived. We ascribe it to the ν(Te=O) stretching.**32**

Thus, from the analysis of the vibrational results we can deduce the coexistence of atomic and molecular oxygen at RT in defected $PtTe_2$. Te vacancies are the only active sites enabling oxygen adsorption at RT. Nevertheless, even in heavily bombarded samples (Pt:Te ratio of 43:57), the attained oxygen coverage is particularly low (0.02 ± 0.01 monolayer, ML), thus indicating a small sticking coefficient for oxygen at RT ($<10^{-4}$).

For the case of defected $PtTe_2$ samples exposed to water at RT, we observed the stable adsorption of H_2O, as evidenced in Figure 4a by the presence of its characteristic vibrational peaks[33] (including the O-H stretching in molecular water at 418 meV) and by the absence of the O-H stretching vibration of isolated -OH groups at 450 meV, which represents an unambiguous fingerprint of the presence of isolated OH groups coming from water decomposition.[33] Water molecules desorb upon heating at 350 K, as evidenced by the disappearance of H_2O-derived modes in the vibrational spectrum (featureless vibrational spectrum in Figure S6, Supporting Information).

As recently reported for Bi_2Se_3,[34] surface doping by carbon atoms (even by trace amounts) represents a powerful tool for tuning the physicochemical properties of the surfaces of layered materials hosting Dirac fermions. Moreover, carbon atoms are the most common residual impurities incorporated in the bulk of single crystals.[35] Thus, it is important to evaluate in details the influence of surface carbon doping on the surface chemical reactivity of $PtTe_2$. Accordingly, we have doped defected samples by carbon atoms by enabling their segregation from the bulk, as checked by Auger electron spectroscopy. Though the presence of carbon in the bulk is rather negligible (see Figure S2, Supporting Information), residual carbon atoms migrate toward the surface after prolonged heating of the samples (1 hour at ≈750 K). These interstitial carbon atoms occupy Te vacancies, so as to obtain substitutional carbon atoms in the near-surface layers with a saturation coverage of 0.01 ML, which corresponds to a surface density of 1.2×10^{-11} g cm^{-2} of carbon atoms.

Remarkably, we observed water decomposition occurring already with an ultralow carbon doping of 0.01 ML. This is clearly revealed by the O-H shoulder at 450 meV, arising from hydroxyl groups, in the corresponding vibrational spectrum (Figure 5a) that coexists with the O-H stretching in molecular water at 418 meV. From the ratio between the spectral components at 418 and 450 meV (see fit procedure in Figure 5c), we can estimate that ≈30% of water molecules are dissociated. Another fingerprint of water decomposition is represented by the C-OH vibration at 155 meV[36] (pink component in Figure 5b). Water decomposition is further confirmed by the emergence of both C-H bending and stretching vibrations at 179 (green component in Figure 5b) and 366 meV[37] (light blue component in Figure 5c), respectively. As a matter of fact, these modes reveal the presence of -H fragments coming from dissociated water.

Upon annealing at 430 K, C-H bending and stretching vibrations are not observed, due to the recombination of H atoms into H_2[37] (Figure S6, Supporting Information).

To further support the conclusions of our experiments, we have built a theoretical model based on density functional theory (DFT) calculations. We have first determined the minimal thickness for which bulk properties are achieved and, moreover, we have evaluated the influence of spin–orbit coupling (SOC). The analysis of the calculated total density of states (DOS) (Figure S7, Supporting Information) and the band structure (Figure S8, Supporting Information) demonstrates that, similar to the case of $PtSe_2$, in $PtTe_2$ the electronic structure exhibits remarkable changes with thickness. In trilayer $PtTe_2$, the electronic structure already resembles that of the bulk (Figures S7b and S8c, Supporting Information). Based on these results, we choose for the modeling of $PtTe_2$ surface a slab of three layers of $PtTe_2$ building blocks, with nine Pt atoms in each layer (top two layers of this slab are shown in **Figure 6**). The inclusion of SOC induces gap opening in monolayer $PtTe_2$ (Figures S7a and S8a, Supporting Information), but the

contribution of SOC is negligible for higher thickness and, especially, in the bulk (see Section S8, Supporting Information, for more details).

In the following, we illustrate the results of our collinear (i.e., without SOC) calculations for bulk $PtTe_2$. In the case of H_2O, the differential enthalpy of adsorption is positive, as well as its differential enthalpy of decomposition (**Table 1**). On the contrary, the differential enthalpy of adsorption for O_2 on pristine $PtTe_2$ surface (Table 1) is negative (with a positive differential enthalpy of decomposition). However, at RT the differential Gibbs free energy of adsorption is positive for both H_2O and O_2 on pristine and undefected $PtTe_2$ (Table 1). Therefore, their adsorption is energetically unfavorable. We note that the value of the differential enthalpy of adsorption for water on bulk $PtTe_2$ is increased compared to the case of monolayer $PtSe_2$.**22** However, the lower flexibility of the outermost $PtTe_2$ surface layer supported by a bulk crystal and also the different electronic structure (monolayer $PtSe_2$ is semiconductor with a gap of ≈1.2 eV**38** while bulk $PtTe_2$ is a semimetal) implies that the H_2O–surface distance is about 14% higher with respect to the case of water adsorbed on monolayer $PtSe_2$.

In details, our model allows an estimation of the energy cost of oxygen decomposition over pristine and undefected $PtTe_2$ of 2.5 eV mol^{-1}, which is a value comparable with the energy cost for oxidation of graphene (about 1.4 eV mol^{-1}).**39** The value of 2.5 eV mol^{-1} corresponds to a temperature of ≈500 K, as experimentally obtained in ref. **40**. Thus, our model indicates that oxidation of defect-free $PtTe_2$ is possible only at temperatures above 500 K, in excellent agreement with experimental evidence from vibrational spectra reported in Figure 3.

Our theoretical model also evaluates the effects of point defects and carbon impurities on the electronic and the atomic structures.

First, we have assessed the effects of Te vacancies. Our theoretical analysis indicates that presence of Te vacancies induces changes of the local atomic structure (Figure 6b) without perceptible contribution to the electronic structure (Figure S7, Supporting Information). Correspondingly, the distance between the physorbed molecule and the $PtTe_2$ surface changes in the nearness of Te vacancies (Table 1). In the $PtTe_2$ surface modified by Te vacancies, physical adsorption of both oxygen and water becomes favorable. Thus, calculations highlight strongly favored adsorption of ambient gases near Te vacancies. We also evaluated if the dissociation of ambient gases is energetically feasible. For the case of oxygen, the theoretical model reveals that decomposition is favorable (Table 1, columns referring to the undoped $PtTe_2$ case) with evident effects on the electronic structure in vicinity of Fermi level (see Figure S9b, Supporting Information). Our model also describes the initial phases of oxidation. As explained in details in Section S6 (Supporting Information), both the presence of Te vacancies and the intercalation of oxygen atoms in the subsurface region play a key role in the formation of an amorphous tellurium-oxide surface phase. Concerning water, the analysis of the differential Gibbs energy reported in Table 1 indicates that water adsorbs molecularly but without decomposition at RT. Thus, the only presence of Te vacancies does not make $PtTe_2$ suitable for catalyzing water splitting and water–gas shift reactions.

We consider in the following the effects of substitutional carbon atoms on surface chemical reactivity. The replacement of Te by C provides noticeable charge redistribution in almost whole surface layer (see Figure S10, Supporting Information) with dramatic changes in the chemical properties. The occurrence of substitutional carbon atoms provides noticeable distortions of local atomic structure (Figure 6c) compared to the pristine $PtTe_2$ (Figure 6a), without significant changes in electronic structure (Figure S7, Supporting Information). In the presence of substitutional carbon atoms, the most energetically favorable configuration is the one with the carbon–adsorbate distances similar or closer to the values of covalent bonds (Table 1, columns referring to carbon-doped $PtTe_2$ case). On $PtTe_2$ all occupied orbitals of Pt and

Te participate in bond formations, with only unoccupied orbitals out of plane. Specifically, we estimate a negative energy cost for water decomposition over substitutional carbon impurities, with a value (−20.9 kJ mol^{-1}) of the same order of the energy required for water evaporation (43 kJ mol^{-1}).**41** Consequently, C-doped $PtTe_2$ is particularly effective for adsorption and decomposition, with potential application in catalysis (water splitting and water–gas shift).

We finally addressed the concurrent presence of substitutional carbon atoms and Te vacancies. In this case, the energy cost for water decomposition becomes −57.5 kJ mol^{-1}. The corresponding values of the differential enthalpy for molecular adsorption of water are −13.8 (only C impurities) and −210.2 (both C impurities and Te vacancies) kJ mol^{-1}, respectively.

Overall, these theoretical results offer the framework for the understanding of the experimental data (XPS and HREELS) reported in Figures **2**-**5**.

Conclusion

We have discovered that $PtTe_2$ can be transformed from a chemically inert material into a catalyst by means of the introduction of defects and surface functionalization. In particular, undefected bulk $PtTe_2$ is inert toward ambient gases at RT. The oxidation of the undefected $PtTe_2$ surface becomes feasible only for temperature higher than 500 K, thus enabling its use in nanoelectronics. The presence of Te vacancies jeopardizes the chemical inertness and, consequently, the ambient stability of $PtTe_2$. Oxygen- and air-exposed samples of defected $PtTe_2$ exhibit a disordered TeO_2-like surface oxide phase. Therefore, the growth of single crystals with minimized amounts of Te vacancies is crucial in order to favor the technological exploitation of this novel transition-metal dichalcogenide hosting type-II Dirac fermions. The use of $PtTe_2$ in catalysis is feasible in systems modified by surface functionalization. The presence of substitutional C atoms induces water decomposition with hydroxyl groups stably adsorbed at RT. Thus, C-doped bulk $PtTe_2$ could be effectively used in catalysis (e.g., in the water splitting and in the water–gas shift reaction).

These findings open new perspectives for the use of functionalized Dirac materials in catalysis.

Experimental Methods

Growth: High-purity Pt (99.99%) foil and Te ingot (99.9999%) were mixed in the ratio of 1:17 and sealed under vacuum in a quartz tube. The quartz tube was heated to 1270 K, dwelled there for 8 h, and slowly cooled at a rate of 3–5 K h^{-1} to 770 K. Subsequently, the excess Te flux was separated by centrifugation. The resulting crystals have typical dimensions of 8 × 8 × 1 mm^3 with the *c*-axis perpendicular to the plates and can be easily cleaved. The structure of the grown crystals was examined by XRD (Bruker D2 PHASER) using Cu Kα radiation (see Figure S1, Supporting Information) and Laue diffraction at RT.

Experimental Methods: The crystalline quality of the surface and its composition were checked in ultrahigh vacuum (UHV) by means of LEED and XPS, respectively. $PtTe_2$ was cleaved in UHV conditions.

XPS experiments were carried out at the High-Energy branch of the Advanced Photoelectric Experiments beamline (APE-HE) of the Elettra-Synchrotron, Trieste, Italy. XPS spectra were recorded with an Omicron EA125 hemispherical electron energy analyzer, by keeping the sample at RT and in normal emission condition. The linearly polarized light was impinging on the sample forming an angle of 45°

with respect to the normal to the surface. To evaluate binding energies of core levels, a Shirley background was subtracted from XPS spectra.

Vibrational experiments on surface chemical reactivity were carried out by means of HREELS. An HREELS spectrometer (Delta 0.5 by Specs GmbH, Germany) was used with an energy resolution in the 2–4 meV range. The primary electron beam energy E_p in vibrational investigations was 3 eV. All vibrational spectra were acquired with the sample kept at RT. To extract vibrational frequencies, an exponential background was subtracted from each HREELS spectrum.

Air exposure was carried out by keeping the sample in ambient atmosphere.

Theoretical Methods: The atomic structure and energetics of various configurations of various gases on $PtTe_2$ were studied by DFT using the QUANTUM-ESPRESSO code**42** and the GGA-PBE + van der Waals (vdW) approximation, feasible for the description of the adsorption of molecules on surfaces.**43**, **44** Energy cutoffs of 25 and 400 Ry were used for the plane-wave expansion of the wave functions and the charge density, respectively, and the 4 × 4 × 3 Monkhorst–Pack *k*-point grid for the Brillouin sampling.**45**

Physisorption enthalpies were calculated by the standard formula

$$\Delta H_{phys} = \left[E_{host+mol} - (E_{host} + E_{mol})\right] \quad (1)$$

where E_{host} is the total energy of pristine surface, and E_{mol} is the energy of the single molecules of selected species in empty box. In the case of water adsorption, only the gaseous phase was considered. Chemisorption energy is defined as difference between the total energy of the system with adsorbed molecule and the total energy of same system after decomposition of the same molecule on the surface. For the case of physisorption, differential Gibbs free energy was also evaluated by the formula

$$\Delta G = \Delta H - T\Delta S \quad (2)$$

where T is the temperature and ΔS is the change of entropy of adsorbed molecule, which was estimated considering the gas→liquid transition by the standard formula

$$\Delta S = \Delta H_{vaporization} / T \quad (3)$$

where $\Delta H_{vaporization}$ is the measured enthalpy of vaporization.

Calculations for C-doped $PtTe_2$ were performed for the supercell reported in Figure S10 (Supporting Information), for which one carbon atom per 27 atoms in the supercell is present ($Pt_9Te_{17}C$).

References

[1] See recent reviews and references therein: a) Spin-Crossover Materials, Properties and Applications (Ed.: M. A. Halcrow), Wiley, Hoboken, 2013; b) P. Gîtlich, A. B. Gaspar, Y. Garcia, Beilstein J. Org. Chem.

2013, 9, 342–391; c) Special Issue: “Spin- Crossover Complexes” (Eds.: K. S. Murray, H. Oshio, J. A. Real), Eur. J. Inorg. Chem. 2013, 574–1067; d) A. Bousseksou, G. Molnar, L. Salmon, W. Nicolazzi, Chem. Soc. Rev. 2011, 40, 3313–3335; e) Topics in Current Chemistry, Vol. 233–235 (Eds.: P. Gîtlich, H. A. Goodwin), Springer, Berlin, 2004.

[2] a) O. Kahn, C. J. Martinez, Science 1998, 279, 44–48; b) Y. Garcia, V. Ksenofontov, P. Gîtlich, Hyperfine Interact. 2002, 139–140, 543–551; c) J.-F. L¦tard, P. Guionneau, L. Goux-Capes, Top. Curr. Chem. 2004, 235, 221–249; d) G. Moln.r, L. Salmon, W. Nicolazzi, F. Terki, A. Bousseksou, J. Mater. Chem. C 2014, 2, 1360–1366.

[3] I.Sˇ alitrosˇ, N. T. Madhu, R. Bocˇa, J. Pavlik, M. Ruben, Monatsh. Chem. 2009, 140, 695–733.

[4] C. Jay, F. Groliere, O. Kahn, J. Krçber, Mol. Cryst. Liq. Cryst. 1993, 234, 255 –262.

[5] a) S. Bonhommeau, G. Moln.r, A. Galet, A. Zwick, J.-A. Real, J. J. McGarvey, A. Bousseksou, Angew. Chem. Int. Ed. 2005, 44, 4069–4073; Angew. Chem. 2005, 117, 4137–4141; b) S. Cobo, D. Ostrovskii, S. Bonhommeau, L. Vendier, G. Molnar, L. Salmon, K. Tanaka, A. Bousseksou, J. Am. Chem. Soc. 2008, 130, 9019 – 9024.

[6] a) S. Decurtins, P. Gîtlich, C. P. Kçhler, H. Spiering, A. Hauser, Chem. Phys. Lett. 1984, 105, 1–4; b) A. Hauser, Top. Curr. Chem. 2004, 234, 155 –198; c) J.-F. L¦tard, G. Chastanet, P. Guionneau, C. Desplanches in Spin-Crossover Materials, Properties and Applications (Ed.: M. A. Halcrow), Wiley, Hoboken, 2013, pp. 475–506.

[7] a) P. Gîtlich, A. Hauser, H. Spiering, Angew. Chem. Int. Ed. Engl. 1994, 33, 2024–2054; Angew. Chem. 1994, 106, 2109–2141; b) J.-F. L¦tard, P. Guionneau, O. Nguyen, J. S. Costa, S. Marc¦n, G. Chastanet, M. Marchivie, L. Goux-Capes, Chem. Eur. J. 2005, 11, 4582–4589; c) J. K. McCusker, A. L. Rheingold, D. N. Hendrickson, Inorg. Chem. 1996, 35, 2100–2112; d) P. Stock, T. Pe¸dzin´ ski, N. Spintig, A. Grohmann, G. Hçrner, Chem. Eur. J. 2013, 19, 839–842.

[8] C. Roux, J. Zarembowitch, B. Gallois, T. Granier, R. Claude, Inorg. Chem. 1994, 33, 2273–2279.

[9] M.-L. Boillot, J. Zarembowitch, A. Sour, Top. Curr. Chem. 2004, 234, 261–276.

[10] S. Venkataramani, U. Jana, M. Dommaschk, F. D. Sonnichsen, F. Tuczek, R. Herges, Science 2011, 331, 445–448.

[11] Molecular Switches, Vol. 1–2 (Eds.: B. L. Feringa, W. R. Browne), Wiley-VCH, Weinheim, 2011.

[12] M. Milek, F. W. Heinemann, M. M. Khusniyarov, Inorg. Chem. 2013, 52, 11585–11592.

[13] a) A. Tissot, M.-L. Boillot, S. Pillet, E. Codjovi, K. Boukheddaden, L. M. L. Daku, J. Phys. Chem. C 2010, 114, 21715–21722; b) Y. Hasegawa, K. Takahashi, S. Kume, H. Nishihara, Chem. Commun. 2011, 47, 6846–6848; c) K. Takahashi, Y. Hasegawa, R. Sakamoto, M. Nishikawa, S. Kume, E. Nishibori, H. Nishihara, Inorg. Chem. 2012, 51, 5188–5198.

[14] M. Nihei, Y. Suzuki, N. Kimura, Y. Kera, H. Oshio, Chem. Eur. J. 2013, 19, 6946–6949.

[15] V. W.-W. Yam, C.-C. Ko, N. Zhu, J. Am. Chem. Soc. 2004, 126, 12734–12735.

[16] M. Morimoto, M. Irie, Chem. Commun. 2005, 3895–3905.

[17] The corresponding spectra obtained in acetonitrile solution under similar conditions are provided in Supporting Information.

[18] F. Terzi, L. Pasquali, M. Montecchi, S. Nannarone, A. Viinikanoja, T. o.ritalo, M. Salom.ki, J. Lukkari, B. P. Doyle, R.

Seeber, J. Phys. Chem. C 2011, 115, 17836–17844.

[19] A long irradiation time was chosen to guarantee that the photostationary state (PSS) was reached. Although the photon flux in XPS/NEXAFS experiments was substantially smaller than in photoswitching experiments monitored by electronic absorption spectroscopy, it is likely that the PSS state was reached before the end of the irradiation time of 8–12 h.

[20] B. Warner, J. C. Oberg, T. G. Gill, F. E. Hallak, C. F. Hirjibehedin, M. Serri, S. Heutz, M.-A. Arrio, P. Sainctavit, M. Mannini, G. Poneti, R. Sessoli, P. Rosa, J. Phys. Chem. Lett. 2013, 4, 1546 – 1552.

[21] M. Bernien, D. Wiedemann, C. F. Hermanns, A. Krîger, D. Rolf, W. Kroener, P. Mîller, A. Grohmann, W. Kuch, J. Phys. Chem. Lett. 2012, 3, 3431–3434.

[22] M. Irie, T. Fukaminato, K. Matsuda, S. Kobatake, Chem. Rev. 2014, 114, 12174–12277.

[23] The time constants obtained from the NEXAFS data should be taken with care due to possible fluctuations of X-ray intensity during the experiment.

[24] a) M. S. Alam, M. Stocker, K. Gieb, P. Mîller, M. Haryono, K. Student, A. Grohmann, Angew. Chem. Int. Ed. 2010, 49, 1159 – 1163; Angew. Chem. 2010, 122, 1178–1182; b) A. Rotaru, I. A. Gurallskiy, G. Molnar, L. Salmon, P. Demont, A. Bousseksou, Chem. Commun. 2012, 48, 4163–4165; c) E. Ruiz, Phys. Chem. Chem. Phys. 2014, 16, 14 –22.

[25] a) E. A. Osorio, K. Moth-Poulsen, H. S. J. van der Zant, J. Paaske, P. Hedeg.rd, K. Flensberg, J. Bendix, T. Bjørnholm, Nano Lett. 2010, 10, 105–110; b) V. Meded, A. Bagrets, K. Fink, R. Chandrasekar, M. Ruben, F. Evers, A. Bernand-Mantel, J. S. Seldenthuis, A. Beukman, H. S. J. van der Zant, Phys. Rev. B 2011, 83, 245415.

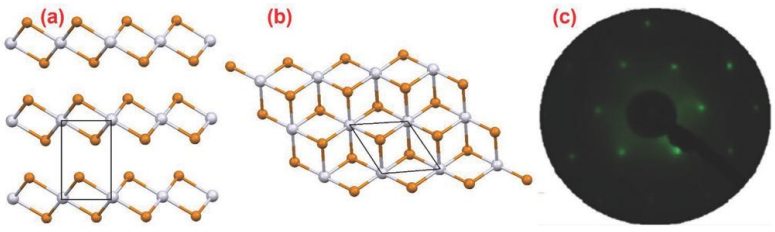

Figure 1: a) Side and b) top views of the crystal structure of $PtTe_2$. Light brown balls denote Te atoms, while Pt is represented by white-gray balls. The unit cell is indicated by black lines. c) The LEED pattern acquired at a primary electron beam energy of 72 eV.

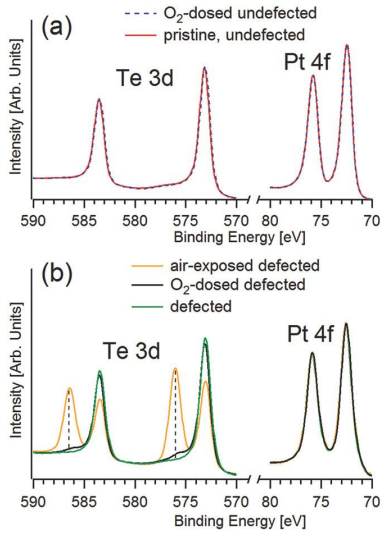

Figure 2: High-resolution XPS spectra of Pt-4f and Te-3d core levels taken for: a) the pristine $PtTe_2$ sample (red curve) and the same surface exposed to 10^6 L of O_2 (dashed blue curve); b) defected $PtTe_2$ (green curve), the same surface exposed to 10^6 L of O_2 (black curve) and air-exposed defected $PtTe_2$ (yellow curve). Note that the line-shape of Pt-4f core levels overlaps for all spectra reported in both panels, while Te 3d core levels coincide in spectra in panel (a) but their respective line-shape differs in the cases shown in panel (b). For all spectra, the photon energy is 745 eV and the energy resolution is 0.1 eV.

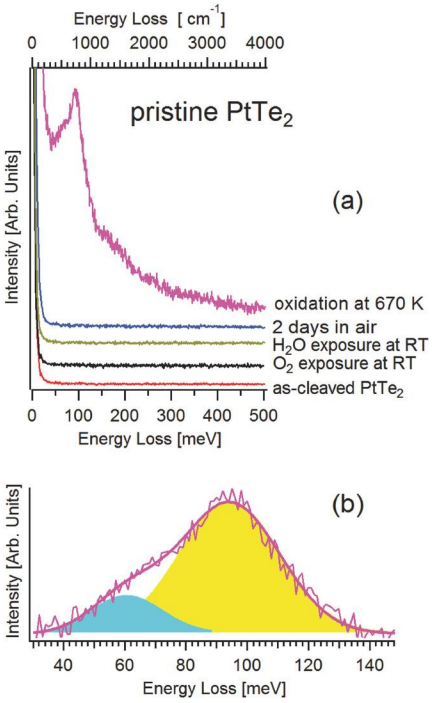

Figure 3: a) Vibrational spectra for as-cleaved $PtTe_2$ and for the same surface exposed to 10^3 L of O_2 and H_2O at RT. Successively, the surface has been exposed to air. No vibrational peak is observed. Contrarily, upon oxidation at 600 K the vibrational spectrum exhibits features arising from surface oxidation. b) The fitting procedure of the latter spectrum is reported.

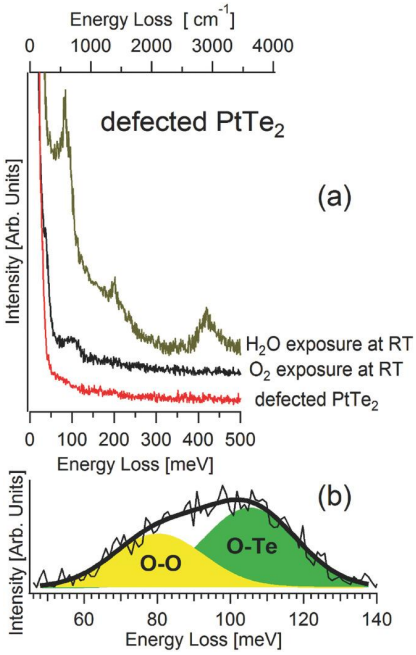

Figure 4: a) Vibrational spectra for $PtTe_2$ modified with the implantation of defects (Te vacancies) by means of Ar-ion bombardment. The obtained surface has been successively exposed to 10^3 L of O_2 and H_2O at RT. b) The results of a fitting procedure for the vibrational spectrum of the O_2-dosed $PtTe_2$ revealing spectral contributions from O-O (yellow area) and O-Te (green area), respectively.

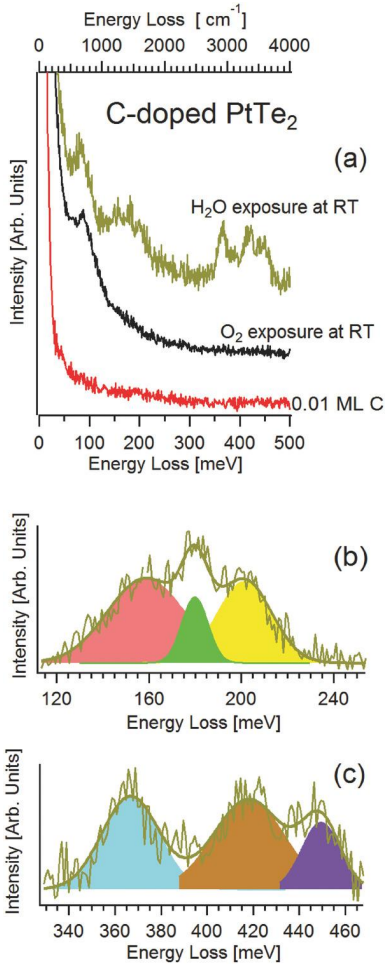

Figure 5: a) Vibrational spectra for $PtTe_2$ modified by doping with 0.01 ML of carbon atoms. The C-doped sample has been successively exposed to 10^3 L of O_2 and H_2O at RT. For the latter case, a fitting procedure has been performed, whose results are reported in panels (b) and (c). b) Spectral contributions from C-OH (pink area), C-H stretching (green area), and scissoring (yellow area) vibrations are evidenced, respectively. While the first two modes are related to -OH and -H fragments arising from water decomposition, the latter feature is the scissoring vibration of molecular water. c) Spectral contributions from C-H stretching (light blue area), O-H in molecular water (brown area), and O-H in isolated -OH groups (purple area) are evidenced, respectively.

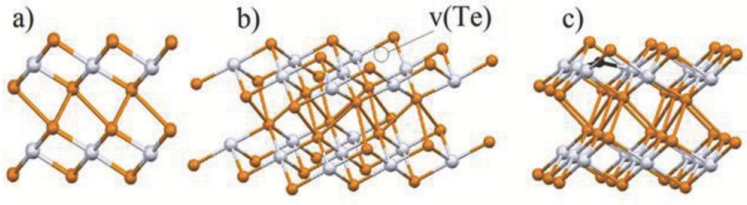

Figure 6: Optimized atomic structure of a) pristine and c) carbon-doped $PtTe_2$ supercell, while panel b) shows the case in which the atomic structure is modified by the presence of one Te vacancy. White, light brown, and black balls represent Pt, Te, and C atoms, respectively. The Te vacancy is evidenced in panel (b) by an empty circle and by the annotation "v(Te)."